

Organic & Biomolecular Chemistry

Accepted Manuscript



This is an *Accepted Manuscript*, which has been through the Royal Society of Chemistry peer review process and has been accepted for publication.

Accepted Manuscripts are published online shortly after acceptance, before technical editing, formatting and proof reading. Using this free service, authors can make their results available to the community, in citable form, before we publish the edited article. We will replace this *Accepted Manuscript* with the edited and formatted *Advance Article* as soon as it is available.

You can find more information about *Accepted Manuscripts* in the [Information for Authors](#).

Please note that technical editing may introduce minor changes to the text and/or graphics, which may alter content. The journal's standard [Terms & Conditions](#) and the [Ethical guidelines](#) still apply. In no event shall the Royal Society of Chemistry be held responsible for any errors or omissions in this *Accepted Manuscript* or any consequences arising from the use of any information it contains.

Mechanistic studies for tri-targeted inhibition of enzymes involved in cholesterol biosynthesis by green tea polyphenols

Hu Ge^{1,#}, Jinggong Liu^{1,#}, Wenxia Zhao², Yu Wang¹, Qingqing He¹, Ruibo Wu¹, Ding Li^{1,*} and Jun Xu^{1,*}

¹ School of Pharmaceutical Sciences & Institute of Human Virology, Sun Yat-Sen University, 132 East Circle Road at University City, Guangzhou, 510006, China.

² Department of Pharmacy, The Sun Yat-sen Memorial Hospital of Sun Yat-sen University, Guangzhou 510120, China

#Authors with equal contributions.

*Correspondence to: junxu@biochemomes.com (J. Xu), liding@mail.sysu.edu.cn (D. Li)

Abstract: In the present study, we found that three enzymes, MVK, MDD, and FPPS, in mevalonate pathway (MVP) of cholesterol biosynthesis, can be simultaneously inhibited by two green tea polyphenols ((-)-epicatechin-3-gallate, ECG; (-)-epigallocatechin-3-gallate, EGCG). Molecular dynamics simulations and pharmacophore studies were carried out to elucidate the tri-targeted inhibition mechanisms. Our results indicate that similar triangular binding pockets exist in all these three enzymes, which is essential for their binding with polyphenols. Two distinct binding poses for ECG and EGCG were observed in our MD simulations. These results shed light on further selective and multi-targeted inhibitor design for treatment of hyperlipidemia.

Keywords: anti-hyperlipidemia; MD simulations; pharmacophore modeling; tri-targeted inhibition; mevalonate pathway.

Abbreviations: 3D, three-dimensional; FPPS, farnesylpyrophosphate synthase; MD, molecular dynamics; MDD, mevalonate 5-diphosphate decarboxylase (also known as mevalonate 5-pyrophosphate decarboxylase or MPD); MVK, mevalonate kinase;

1. Introduction

Green tea has been consumed for centuries and has sparked growing interest in its potential health benefit.¹ Green tea mainly contains polyphenols, such as (+)epicatechin (EC), (-)epigallocatechin (EGC), (-)epicatechin-3-gallate (ECG), and (-)epigallocatechin-3-gallate (EGCG)² (Fig. 1). Studies report that green tea reduces the risks of cancer,³⁻⁶ cardiovascular diseases,⁷⁻⁹ neurodegenerative diseases,¹⁰ diabetes,¹¹ and obesity.¹²⁻¹⁴ Further studies indicate that green tea polyphenols lower serum cholesterol in animals or human¹⁵⁻¹⁸, and suppress hepatic cholesterol synthesis through inhibiting HMG-CoA reductase¹⁹ and squalene epoxidase,²⁰ which are the rate-limiting enzymes in *in vivo* cholesterol biosynthesis.²¹ Therefore, it is necessary to identify which green tea polyphenols could reduce cholesterol levels and elucidate the inhibitory mechanism.

Mevalonate pathway contains a unique series of three sequential ATP-dependent enzymes that convert mevalonate to isopentenyl diphosphate (IPP): mevalonate kinase (MVK), phosphomevalonate kinase (PMK), and mevalonate 5-diphosphate decarboxylase (MDD). Several investigators have suggested the involvement of these three enzymes as important regulatory steps in the biosynthesis of cholesterol.

Mevalonate kinase (MVK), the fourth enzyme of the mevalonate pathway, catalyzes a nucleophilic attack by a C5 anion of mevalonate on the γ -phosphate of ATP forming mevalonate-5-phosphate.²² This irreversible reaction requires a divalent cation and represents a key step in the production of polyisoprenoid and sterol metabolites from acetate. The significance of MVK has been further highlighted by the implication of the enzyme in human inherited diseases, such as mevalonic aciduria and hyperimmunoglobulinemia D/periodic fever syndrome.^{23, 24}

Mevalonate pyrophosphate decarboxylase (MDD) catalyzes the ATP dependent decarboxylation of mevalonate 5-diphosphate (MVAPP) to form isopentenyl

5-diphosphate (IPP), inorganic phosphate (Pi), ADP, and CO₂.^{25, 26} Inhibition of this enzyme effectively diminishes biosynthesis of cholesterol, and low MDD activity correlates with decreased cholesterol levels in a hypertensive rat strain.^{25, 27}

Farnesyl pyrophosphate synthase (FPPS) is a key regulatory enzyme in the mevalonate pathway.²⁸ The enzyme that catalyzes the consecutive head-to-tail condensations of isopentenyl diphosphate (IPP) and dimethylallyl diphosphate (DMAPP) to form C10 geranyl diphosphate (GPP) and subsequently C15 farnesyl diphosphate (FPP). Pyrophosphate (PPi) is generated as the byproduct of the reaction (Figure 1.39).²⁹ A distinct enzyme further elongates FPP by condensation with an additional molecule of isopentenyl diphosphate to produce C20 geranylgeranyl diphosphate (GGPP). FPP and GGPP are precursors for the biosynthesis of most of the isoprenoid compound family. Importantly, FPP and GGPP are the branching point in the mevalonate pathway leading to prenylated proteins and to the biosynthesis of dolichols and sterols, such as cholesterol and ergosterol.³⁰

Herein, we found that green tea polyphenols, ECG and EGCG, could inhibit three enzymes (FPPS, MVK, and MDD) of the mevalonate pathway essential for *in vivo* cholesterol biosynthesis. In contrast, other green tea components, EC and EGC, had no such effects. Molecular modeling on receptor-ligand complexes was performed to reveal the ligand binding modes of FPPS, MVK, and MDD. Pharmacophore models were built for analyzing the protein-ligand interactions. The present study will help to discover new cholesterol lowering agents, and inspire designing of multiple-target inhibitors against other drug targets.

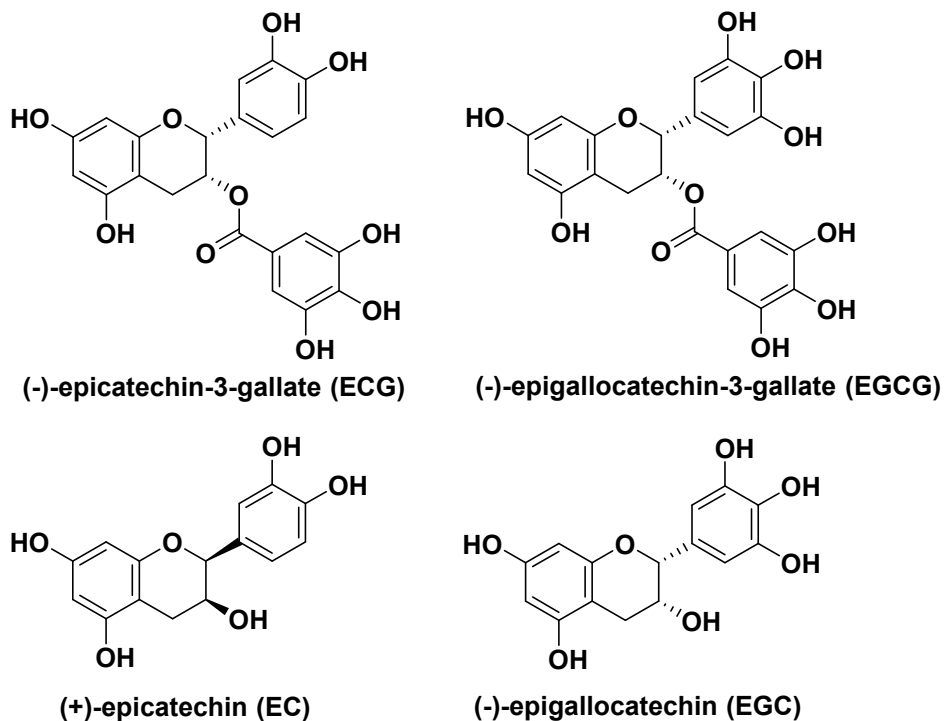


Figure 1. The structures of four major components of green tea polyphenols

2. Results and discussion

2.1. The ECG and EGCG of green tea polyphenols showed micromolar *in vitro* inhibition against FPPS, MVK, and MDD

Three cholesterol-related enzymes (FPPS, MVK, and MDD) were purified to apparent homogeneity as potential drug targets for green tea polyphenol inhibition studies. Four compounds (ECG, EGCG, EC and EGC) were tested against these enzymes with enzyme activity inhibitory assays and fluorescence titration assays. The IC_{50} and K_d values for each compound were determined (Table 1). Both ECG and EGCG showed micro molar inhibition to all three enzymes (FPPS, MVK and MDD), while EC and EGC were unable to inhibit these three enzymes. It is possibly because ECG and EGCG all have the galloyl

group, which is important for their activity, but not included in EC and EGC.

Table 1. IC₅₀ and K_d values for enzyme inhibition by green tea polyphenols

| Compound | IC ₅₀ (μM) ^a | | | K _d (μM) ^a | | |
|----------|------------------------------------|-----------|------------|----------------------------------|-----------|------------|
| | FPPS | MVK | MDD | FPPS | MVK | MDD |
| ECG | 0.95±0.22 | 5.82±0.29 | 4.48±0.20 | 2.14±0.44 | 7.40±1.12 | 6.62±0.34 |
| EGCG | 1.96±0.13 | 5.51±0.07 | 13.36±0.15 | 6.10±0.38 | 5.29±0.48 | 11.44±0.96 |
| EC | >100 | >100 | >100 | >100 | >100 | >100 |
| EGC | >100 | >100 | >100 | >100 | >100 | >100 |

a. The IC₅₀ (μM) values and the K_d values shown are the mean ± SD of three experiments.

2.2. Rat FPPS, MVK, and MDD have high homology with corresponding human enzymes

The major purpose of developing cholesterol lowering agents should be lowering cholesterol levels for human patients. Therefore, we compared the similarity of human and rat FPPS, MDD, and MVK enzymes, from the aspects of both sequence and structure. Due to the lack of crystal structures for rat FPPS and MDD, we built homology models for both of them. Then, the sequence identity and structural RMSDs between human and rat enzymes were calculated, respectively. Table 2 lists the percent identities between human and rat protein sequences of FPPS, MDD, and MVK. All the identities are >80%, indicating that they have high homology. Figure 2 depicts the structures of human and rat enzymes and the corresponding RMSDs. All the backbone RMSDs are <1 Å, which means the whole proteins are quite similar. Also, the pocket RMSDs are even smaller, implying that the ligand binding pockets are more conserved. The high similarity in both protein sequence and 3D structure revealed that rat FPPS, MVK, and MDD have high homology with human. Our experimental results on rat enzymes implies the green tea polyphenols should inhibit human FPPS, MVK, and MDD as well.

Table 2. The 3D structures and homology between human and rat FPPS, MDD, and MVK

| Enzyme | FPPS | MDD | MVK |
|--------------|----------------|----------------|-----------|
| Human | PDB: 3N6K | PDB: 3D4J | PDB: 2R3V |
| Rat | Homology Model | Homology Model | PDB: 2R42 |
| Identity (%) | 84.6 | 84.8 | 81.8 |

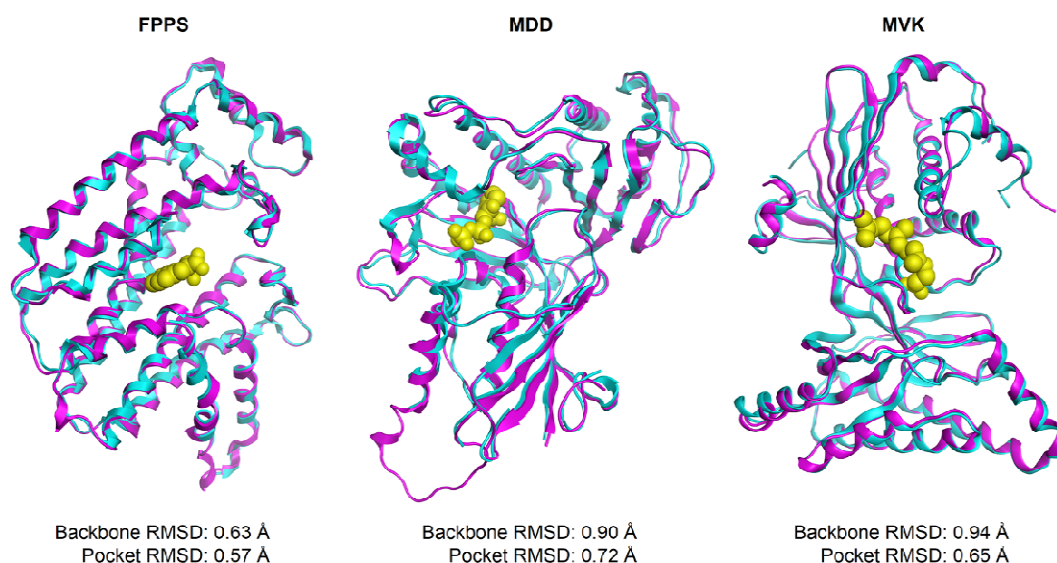


Figure 2. The structural similarity between human and rat source enzymes. The structures from human are in cyan, and those from rats are in magenta.

2.3. Theoretical interaction models by molecular docking and MD simulation

To study the structure-activity relationships between the green tea polyphenols and the three targets, computational studies like molecular docking, molecular dynamics (MD) simulations were performed. Prior to the docking of green tea polyphenols, method assessments were carried out. Generally, there are four ways to analyze the outcome of a docking campaign: (1) The accuracy of the binding pose prediction, (2) the accuracy of

the affinity prediction, (3) the enrichment rates obtained by virtual screening, (4) the diversity of the hit list.³¹ In this study, the purpose of molecular docking is to predict the binding poses of the polyphenols, implying that the accuracy of the binding pose prediction is our major concern. This is usually determined by re-docking of the co-crystal ligand back into the binding site.³² In this study, each native ligand from the three co-crystal structures was docked back into its original binding site using GLIDE, MOE, and CDOCKER, respectively. The results of the re-docking experiments are depicted in Fig. 3, suggesting that GLIDE is the best program for green tea polyphenol docking studies. Therefore, the green tea polyphenols were docked into the binding sites of rat FPPS, MVK, and MDD via GLIDE. For each receptor-ligand complex, 50 ns MD simulation was carried out following solvation.

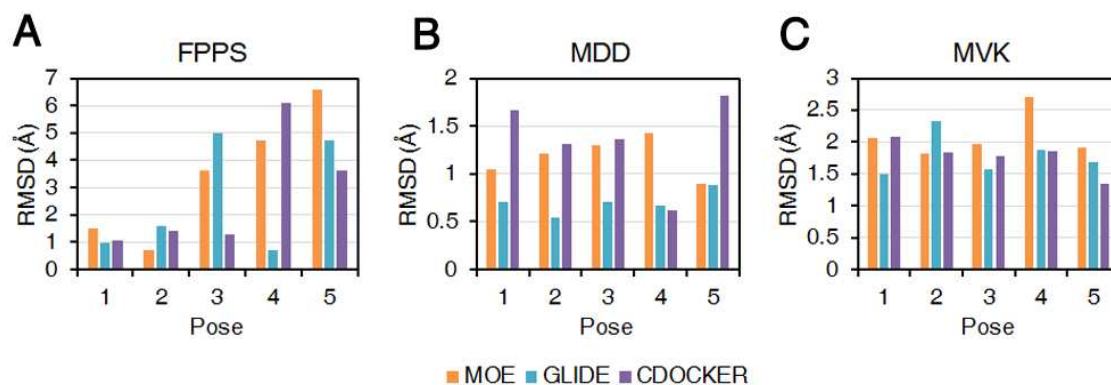


Figure 3. The RMSDs of the top five docked poses and the experimental poses of the co-crystal structures from (A) FPPS, (B) MDD, and (C) MVK. Three docking programs, MOE, GLIDE, and CDOCKER were tested and their RMSD results are colored differently.

2.4. Energetic profiles upon polyphenols binding

The time-dependent RMSDs for the 50 ns production-phase MD of six energetically favorable ligand-complex systems (ECG and EGCG with FPPS, MVK and MDD) are

depicted in Fig. S6 of the Supporting Information, including the RMSDs of the receptor backbone atoms, the binding pocket residues, and the ligands. The majority of RMSDs reached equilibrium within 10 ns, and remained stable during the rest of simulations. Thus, it was reasonable to perform binding energy calculations based on the last halves of trajectories at the equilibrium state.

All the green tea polyphenols' (ECG, EGCG, EC, and EGC) binding affinities to the targets (FPPS, MVK and MDD) were calculated to interpret the assay results of Table 1. The binding energies of ECG and EGCG with FPPS, MVK and MDD are listed in Table 3. The binding energies of EC with FPPS, MVK and MDD are -16.3, -17.6, and -18.7 kcal/mol, respectively; the binding energies of EGC with FPPS, MVK and MDD are -17.0, -7.2, and -18.1 kcal/mol, respectively. However, the binding energies of ECG and EGCG with all three targets are around -30 kcal/mol. These calculations are consistent with the assay results that ECG and EGCG are active while EC and EGC not.

The binding affinities of the active green tea polyphenols (ECG and EGCG) with the targets (FPPS and MDD) mainly come from electrostatic and van der Waals interactions, and the electrostatic interactions contribute more. For MVK, the magnesium ion (Mg^{2+}) was treated with different ways in docking. At first, it was treated as a dummy atom, but the calculated binding affinity between the receptor and the ligands were too weak. When ligand-metal interaction restraints were added (Mg^{2+} treated as an anchor), the binding energy significantly improved and high consistency was observed between the calculation and the bioassay. In this case, the binding affinities with the polyphenols are mainly derived from electrostatic interactions (ligand- Mg^{2+} interactions), and the vdW contribution is relatively minor.

Table 3. The binding energy of ECG and EGCG bound to FPPS, MVK and MDD

| Receptor | FPPS | | MVK | | MDD | |
|----------------------|--------|--------|--------|--------|--------|--------|
| | ECG | EGCG | ECG | EGCG | ECG | EGCG |
| $\Delta E_{VDWAALS}$ | -45.3 | -45.0 | -24.9 | -25.2 | -47.9 | -50.8 |
| ΔE_{ELE} | -101.7 | -99.6 | -298.6 | -273.4 | -84.9 | -98.7 |
| ΔE_{PB} | 90.9 | 89.5 | 266.6 | 243.6 | 73.4 | 88.0 |
| ΔE_{NPOLAR} | -32.9 | -31.0 | -26.8 | -26.5 | -35.7 | -37.8 |
| ΔE_{DISPER} | 57.4 | 55.5 | 47.5 | 48.2 | 66.2 | 68.1 |
| ΔE_{GAS} | -147.0 | -144.6 | -323.5 | -298.6 | -132.9 | -149.6 |
| ΔE_{SOLV} | 115.3 | 114.0 | 287.3 | 265.3 | 103.9 | 118.2 |
| ΔE_{TOTAL} | -31.7 | -30.6 | -36.1 | -33.3 | -29.0 | -31.3 |

^a All energy units are in kcal/mol.

2.5. Key residues for activities and triangular binding modes

To obtain more sights on the interaction between the ligands and receptors, binding energy decompositions were conducted to reveal where the most important interaction energies come from the FPPS, MVK, and MDD. Energy contribution of all residues around 8 Å of the binding sites of FPPS, MVK and MDD were calculated and ten essential residues were identified for each enzyme (Fig. 4). The contribution of each residue was calculated for both EGCG and ECG, and the maximal value was kept.

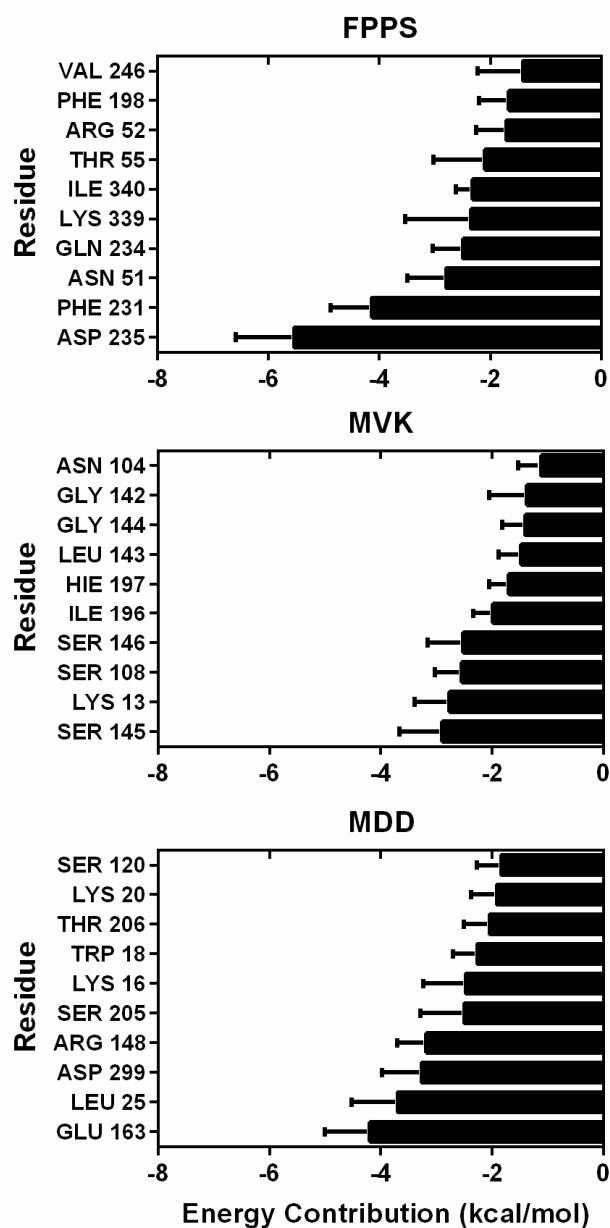


Figure 4. The top ten energetically essential residues of enzymes FPPS, MVK, and MDD and their contributions to the binding energy.

The optimal binding modes of the green tea polyphenols bound to FPPS, MVK and MDD are shown in Fig. 5. ECG and EGCG exhibit quite similar patterns when binding with FPPS and MVK. Here as representatives, only EGCG's optimal binding modes are depicted in Fig. 5A (FPPS with EGCG) and Fig. 5B (MVK with EGCG). However, we

sampled two types of different optimal binding patterns upon binding of EGCG and ECG to MDD, as shown in Fig. 5C and 5D, respectively.

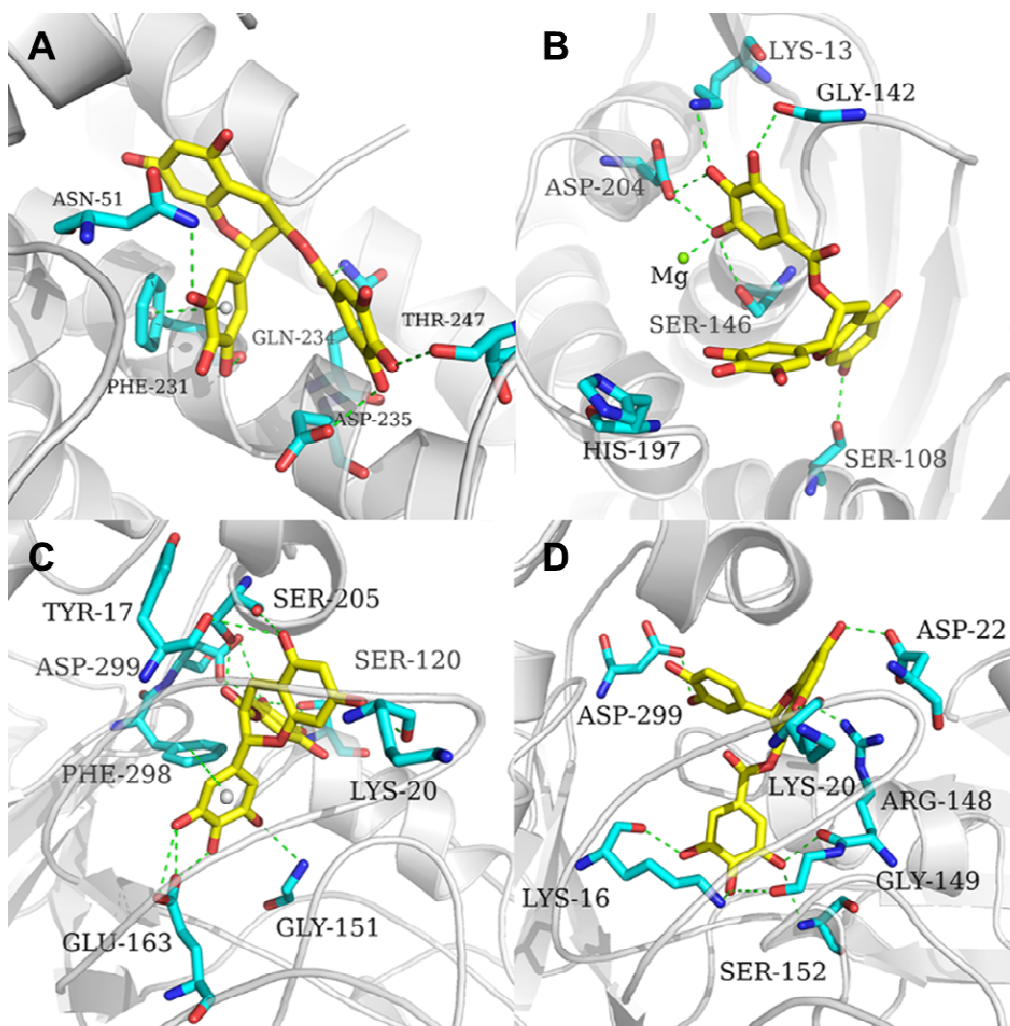


Figure 5. Optimal binding modes of the green tea polyphenols with three targets: (A) FPPS complexed with EGCG (B) MVK complexed with EGCG (C) MDD complexed with EGCG (D) MDD complexed with ECG.

Multiple hydrogen bonds were established in all complexes, benefited from the phenol-rich ligands. Other interactions like π - π stacking interactions at PHE-231 of FPPS (Fig. 5A), PHE-298 of MDD (Fig. 5C) are also observed. Besides, MVK has an Mg^{2+} ion, which forms strong coordination bond with the polyphenol ligands (Fig. 5B). The binding

mode of ECG is quite different from that of ECG when bound to MDD. As depicted in Fig. 5C and 5D, they have two distinct orientations in the same binding pocket. Considering that both orientations are energetically favorable, one inference is that the pocket of MDD is relatively flexible and can accommodate different ligand binding modes. Higher RMSD and RMSF values of MDD partly support this point (Supporting Information).

In summary, the electrostatic and vdW interactions of polyphenols with FPPS, MVK, and MDD are reflected by polar contacts like hydrogen bonding, coordination bonding, and hydrophobic contacts like π - π stacking. Besides, the molecular surfaces of three enzymes were generated to articulate the shapes of the binding pockets when ligands were docked (Fig. 6). The binding pockets of FPPS, MVK, and MDD share following common features: (1) They are all enriched with helices; (2) They all have three sub-sites, which all interact with EGCG or ECG. These three sub-sites are connected to each other and form a triangle.

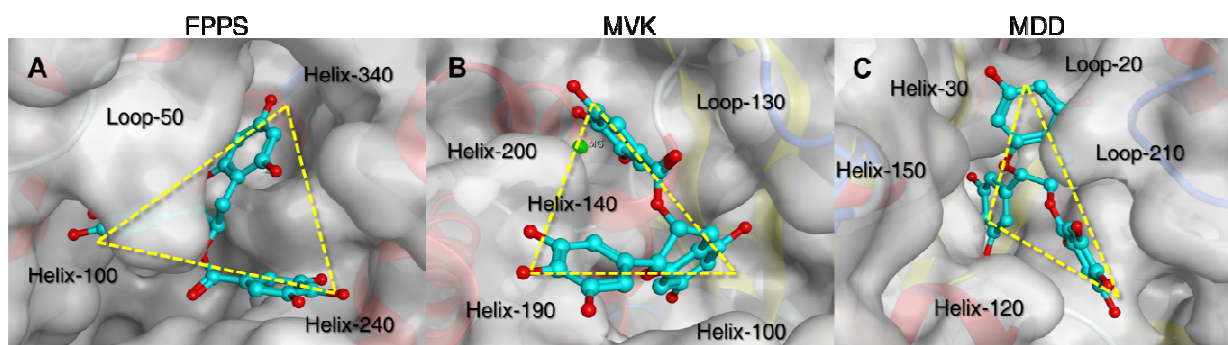


Figure 6. The common features of the FPPS, MVK, and MDD binding pockets, upon EGCG binding. Yellow dash lines connect the three sub-sites.

2.6. Two classes of pharmacophores and target selectivity

Pharmacophore modeling generates hypotheses regarding the binding interactions of a ligand-receptor complex. We have several successful applications of pharmacophore

modeling in previous work.³³⁻³⁵ One pharmacophore may be biased. A consensus pharmacophore, which is more objective, can be considered "the largest common denominator shared by a set of active molecules"(IUPAC 1998).³⁶ To find out the underlying pattern of the triple-target inhibition activity of green tea polyphenols, a pharmacophore consensus method was used to generate the active molecules' common features.

Superimposing active binding poses of ECG and EGCG in the three binding modes (for FPPS, MVK, and MDD) indicates that the poses are divided into two pharmacophore groups: FPPS-class and MVK-class (Fig. 7A). The scaffold of ECG and EGCG consists of the core group, group A, and group B. The group A and B separately connect the core group with two rotatable single bonds (Fig. 7B). The scaffold's conformation can change based upon the receptor's binding pocket. When the group A is perpendicular to the core group, the FPPS-class pharmacophore is formed (Fig. 7C). When the group B is perpendicular to the core group, the MVK-class pharmacophore is generated (Fig. 7D). When ECG binds to MDD, it forms an FPPS-class pharmacophore; when EGCG binds to MDD, it forms an MVK-class pharmacophore. The binding pockets of FPPS and MVK are different, which induces ECG and EGCG to form different pharmacophores. The binding pocket of MDD is flexible enough to accommodate both FPPS-class and MVK-class pharmacophores. The three groups of ECG and EGCG scaffold can freely switch between FPPS-class and MVK-class pharmacophores, so that ECG and EGCG can inhibit all three targets. If a rigid molecule fits either one of the two types of the pharmacophores, the molecule will selectively bind to a specific target. Therefore, the two classes of pharmacophores should be useful for designing, if necessary, selective inhibitors for MVK, FPPS, and MDD.

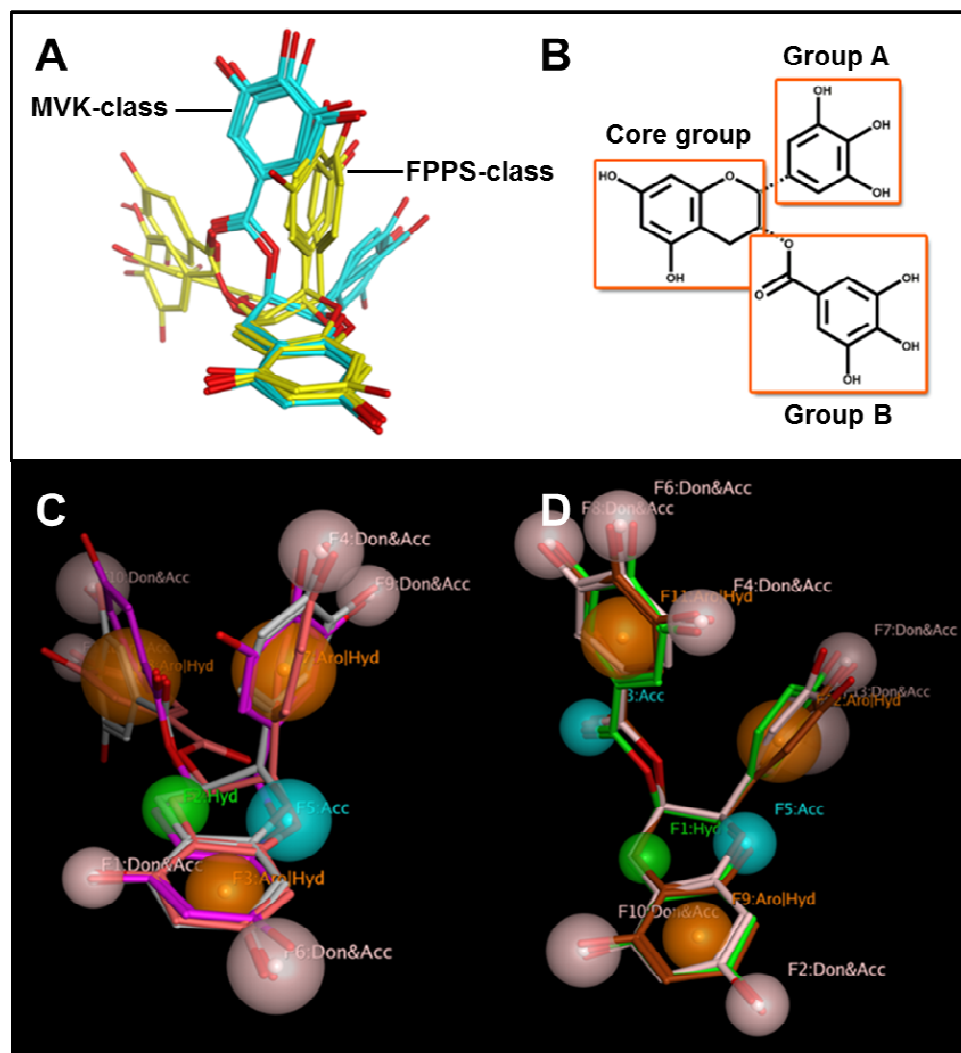


Figure 7. Pharmacophore models generated from superposing the polyphenols' representative binding poses. (A) Superposing ECG and EGCG representative binding poses in the three targets (FPPS, MVK, and MDD). (B) EGCG's three functional groups. (C) Pharmacophore derived from FPPS binding. (D) Pharmacophore derived from MVK binding. Orange: hydrophobic centroids or aromatic centers (Aro|Hyd); Green: hydrophobic centroids (Hyd); Pink: H-bond acceptors and donors (Don&Acc); Cyan: H-bond acceptors (Acc).

To further validate the models for their effectiveness in predicting inhibitory activity

of other molecules and selectiveness in discriminating between the two model classes, an enrichment test was conducted. 20 FPPS inhibitors and 20 MVK inhibitors were collected from literature and databases like Pubchem and BindingDB. Then the two pharmacophore models were used to screen the inhibitors, as well as 5,000 random compounds from Guangdong Small Molecule Tangible Library (GSMTL).³⁷ The enrichment factors for these two models were calculated (Table 4). Both models exhibit high effectiveness in predicting inhibitory activities and high selectivity in discriminating between the two classes. The chemical structures of the known 20 FPPS inhibitors and 20 MVK inhibitors have been supplied in the supplemental information (Figure S8 and S9).

Table 4. Enrichment test results of the two pharmacophore models

| | Number of molecules | Hit rate by FPPS-class model (%) | Hit rate by MVK-class Model (%) |
|-------------------|---------------------|----------------------------------|---------------------------------|
| FPPS inhibitors | 20 | 45 | 15 |
| MVK inhibitors | 20 | 10 | 55 |
| ECG & EGCG | 2 | 100 | 100 |
| Random compounds | 5,000 | 3.7 | 4.1 |
| Enrichment factor | | 12.2 | 13.4 |

The main difference of the two classes of pharmacophores can be reflected by the dihedral angle between the planes of groups A and B. The relation of the dihedral angle and time during 50 ns MD simulations is shown in Fig. 8. For FPPS-ligand complexes, the dihedrals range from 20° to 60°. For MVK-ligand complexes, the dihedrals are around -60°. For MDD-ligand complexes, the dihedrals range from ~60° to 80° for ECG, and -60° to -80° for EGCG. All the dihedral values are stable and have fluctuations of about 20°. This further supports the pharmacophore models.

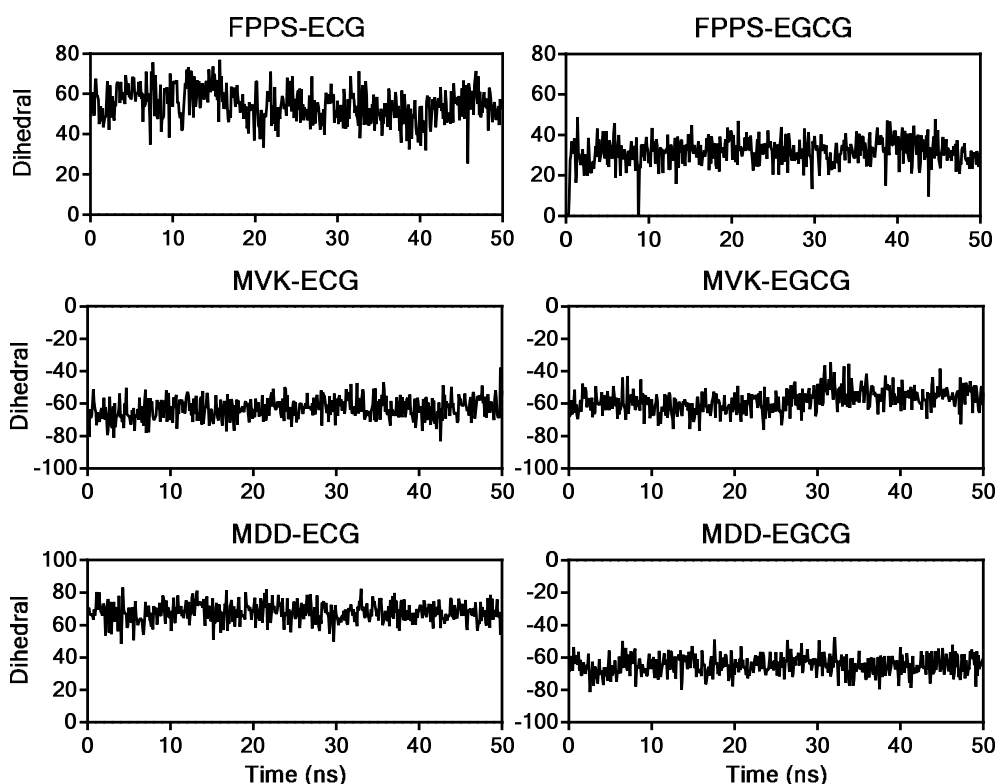


Figure 8. Time dependent dihedral angles between the groups A and B in ECG/EGCG scaffold during 50 ns MD simulations.

3. Experimental

3.1. Enzymes activity inhibitory assay

The green tea polyphenols were obtained from Guangdong Small Molecule Tangible Library (GSMTL), with purity of > 98%. Rat liver MVK, MDD, and FPPS were obtained and assayed as described previously.³⁸⁻⁴⁰ Tris buffer was used instead of phosphate buffer in enzyme storage and assay.

The activity of the ATP-dependent enzymes, MVK and MDD, were assayed spectrophotometrically following a continuous enzyme-coupled assay method.

Determination of IC_{50} for inhibitors of rat mevalonate kinase. At room temperature, rat MVK (1.2 $\mu\text{g}/\text{mL}$) was incubated with or without inhibitor in 100 mM Tris-HCl buffer (pH 7.5) containing 5 mM MgCl_2 , 0.25 mM ATP, 0.5 mM phosphoenol pyruvate, 0.16 mM NADH, 29 unit pyruvate kinase, 37 unit lactic dehydrogenase for 2 minutes, and mevalonate (35 μM) was added to initiate the reaction. IC_{50} was determined by a reciprocal plot of relative activity versus inhibitor concentration (Dixon plot). The intersect of the fitting line with x-axis is equal to IC_{50} in value.

Determination of IC_{50} for inhibitors of rat mevalonate 5-pyrophosphate decarboxylase. At room temperature, rat MDD (1.2 $\mu\text{g}/\text{mL}$) was incubated with or without inhibitor in 100 mM Tris-Cl buffer (pH 7.5) containing 0.25 mM MgCl_2 , 0.5 mM ATP, 0.5 mM phosphoenol pyruvate, 0.16 mM NADH, 29 units pyruvate kinase, 37 units lactic dehydrogenase for 2 minutes, and mevalonate 5-diphosphate (35 μM) was added to initiate the reaction. IC_{50} was determined by a reciprocal plot of relative activity versus inhibitor concentration (Dixon plot). The intersect of the fitting line with x-axis is equal to IC_{50} in value.

FPPS was assayed following our previously established method. Assays were performed in flat bottom, 96-well plates. 100 ng of pure FPPS was incubated with or without inhibitor for 10 min at 37 °C in a final volume of 100 μL buffer, containing 50 mM Tris pH 7.5, 2 mM MgCl_2 , 1 mM DTT, 5 $\mu\text{g}/\text{mL}$ BSA, and 100 $\mu\text{U}/\mu\text{L}$ of inorganic pyrophosphatase were added to each well and then the substrates were added to start the reaction. Assays were terminated by the addition of 10 μL of 2.5% ammonium molybdate reagent (in 5 N H_2SO_4), 10 μL of 0.5 M 2-mercaptoethanol and 5 μL of Eikonogen reagent (0.25 g of sodium sulfite and 14.7 g of meta-bisulfite were dissolved in 100 mL water). The mixtures in plates were incubated with gentle mixing on a plate shaker for 20 min. The absorbance was measured at 830 nm using a Microplate Reader. IC_{50} was determined by a reciprocal plot of relative activity versus inhibitor concentration (Dixon plot). The

intersect of the fitting line with x-axis is equal to IC_{50} in value.

3.2. Fluorescence titration assay

Rat liver MVK, MDD, and FPPS contain tyrosines and tryptophans, which contribute to the fluorescence absorbance of enzymes. The binding of small molecules to these enzymes may result in changes to the hydrophilic and hydrophobic environment around said amino acids; such changes can be detected through fluorescence absorbance changes. Our fluorescence titration assay was carried out following a reported protocol (with minor modifications).⁴¹ The assay was carried out in 50 mM Tris buffer, pH 7.4, 5% glycerol, and 5 mM β -mercaptoethanol. The excitation wavelength used in these experiments was 279 nm. Emission spectra were scanned from 300 to 600 nm, with a 5 nm slit width. For data analysis, the values measured for bound probe at the fluorescent emission peak of 538~540 nm were corrected for free compounds/buffer and for any scattering occurred. These corrected fluorescence enhancement or reduction data were used to plot against concentrations of compounds, and analyzed by nonlinear regression to yield dissociation constants (K_d) and extrapolated maximum fluorescence intensity (F_{max}). K_d values were estimated by fitting the titration data to the equation $Y = [F_{max}(X)]/[K_d + (X)]$.

3.3. Homology modeling

Template crystal structures were downloaded from RCSB Protein Data Bank (PDB ID: 3N6K and 3D4J). Target sequences were searched using NCBI BLAST and selected by identity score. The whole modeling process was done in MOE 2012.10. First, ten independent intermediate models were built. These different homology models were the

result of the permutational selection of different loop candidates and side chain rotamers. Then, the intermediate model which scored best according to the GB/VI scoring function was chosen as the final model, subject to further energy minimization using the AMBER12/EHT force field. The Ramachandran plot (Fig. S5) of the final homology models was plotted to help determine whether the homology model is in good shape: most residues should be in favorable or allowable areas, and none of the outliers should be around the ligands' binding site. The Ramachandran plots of the homology models of FPPS and MDD are shown in supplementary Fig. S5.

3.4. Molecular docking

The chemical structures of EC, EGC, ECG, and EGCG were generated using ChemBioDraw13.0. These initial structures were optimized with the MMFF94⁴² force field to obtain the lowest energy conformations, which were used for the following docking. All the green tea polyphenols were docked into the binding pockets of FPPS, MVK, and MDD by using GLIDE, respectively. The ligands in the proteins' binding pockets were removed. The ligands' positions were selected as the binding sites for docking. Default parameters were used with minor modifications. For GLIDE, the XP (extra precision) mode was used. For MOE, the AMBER12/EHT force field and GBVI/WSA dG refinement were used. For CDOCKER, the random conformations were increased to 30. Pose cluster radius was turned on and set to 0.5 Å to avoid generating highly similar poses. The docked poses were ranked with built-in scoring functions, and the root-mean-square deviations (RMSDs) with the original ligands of the co-crystal structures were respectively calculated. Lower RMSDs represent more consistency between predicted and experimental binding modes.

3.5. Molecular dynamics simulations

The ligand-receptor complexes were prepared with the molecular modeling package MOE 2012.10.⁴³ And then the AMBER ff03 force field was applied for each protein. For each protein target, the top three docked poses of a compound were selected as initial conformations for following MD simulations, respectively. Meanwhile, the ligands were optimized at the HF/6-31G(d) level by Gaussian 09 package,⁴⁴ and the partial atomic charges of the ligands were obtained from the restrained electrostatic potential (RESP) charge at the same theoretical level. While the force field parameters of these ligands were generated from AMBER GAFF force field.⁴⁵ Finally, the ligand-receptor complexes were neutralized by adding sodium/chlorine counter ions, and solvated in an octahedral box of TIP3P⁴⁶ water molecules with solvent layers 10 Å between the box edges and solute surface.

All MD simulations were performed using AMBER 12,^{47,48} via protocols described in our previous study⁴⁹ with minor modifications. The SHAKE⁵⁰ algorithm was used to restrict all covalent bonds involving hydrogen atoms with a time step of 2 fs. The Particle mesh Ewald (PME) method⁵¹ was employed to treat long-range electrostatic interactions. For each ligand-receptor system, three steps of minimization were performed before the heating step. First, all atoms in the receptor-ligand complex were restrained with 50 kcal/(mol·Å²), whereas solvent molecules were not restrained. Then, all heavy atoms were restrained with 10 kcal/(mol·Å²) during the minimization steps. The final non-restrained minimization step included 5,000 cycles of steepest descent and 5,000 cycles of conjugated gradient minimization. After the energy minimizations, the whole system was first heated from 0 to 300 K in 50 ps using Langevin dynamics at a constant volume and, then, equilibrated for 400 ps at a constant pressure of 1 atm. A weak constraint of 10 kcal/(mol·Å²) was used to restrain all the heavy atoms in the receptor-ligand complexes

during the heating steps. Periodic boundary dynamics simulations were carried out for the whole system with an NPT (constant composition, pressure, and temperature) ensemble at a constant pressure of 1 atm and 300 K in the production step. Each receptor-ligand solution complex was simulated for 50 ns; 100 snapshots were derived from the equilibrium state of each trajectory (25 to 50 ns) and used for calculating binding energies via MMPBSA.py.⁵²

3.6. Binding energy calculations

The MM/PBSA method⁵³ in the AmberTools suite was used to calculate the binding energies between the ligands and the receptors. For each system, three trajectories were generated through MD simulations from the initial three docked compound poses. Every trajectory was analyzed and the one with the lowest binding energy was selected as the representative binding energy. The conformations from the low energy trajectories of each compound were clustered by using the Ptraj module of AmberTools 12. A representative conformation of a major cluster was extracted from each trajectory and presented for later binding mode visualization. The binding modes were depicted with PyMOL v1.5.0.3. An in-house PyMOL plugin PiViewer was used to detect and annotate the π - π stacking interactions between the ligands and receptor residues.

The free energy of binding, $\Delta G_{\text{binding}}$, was calculated using Eq. (1) from the free energy of the receptor-ligand complex (G_{cpx}) with respect to the unbound receptor (G_{rec}) and ligand (G_{lig}):

$$\Delta G_{\text{binding}} = G_{\text{cpx}} - (G_{\text{rec}} + G_{\text{lig}}) \quad (1)$$

The MM-PBSA (Molecular Mechanics-Poisson-Boltzmann/Surface Area) methodology allows the calculation of the complete binding reaction energy, including the desolvation of the ligand and the unbound protein, on the basis of a thermodynamic

cycle. Therefore, Eq. (1) can be approximated as

$$\Delta G_{\text{binding}} = \Delta E_{\text{MM}} - T\Delta S + \Delta G_{\text{sol}} \quad (2)$$

$$\Delta E_{\text{MM}} = \Delta E^{\text{ele}} + \Delta E^{\text{vdw}} \quad (3)$$

All energies expressed in the above equations were averaged over the course of the molecular dynamics trajectories. In Eq. (3), ΔE_{MM} is the molecular mechanical energy obtained from the electrostatic (ΔE^{ele}) and the van der Waals (vdW, ΔE^{vdw}) interactions within the system. Here, $T\Delta S$ is the solute entropic contribution at temperature T (kelvin) and the solvation free energy (ΔG_{sol}) represents the electrostatic and nonpolar free energy of solvation, and therefore can be expressed as

$$\Delta G_{\text{sol}} = \Delta G_{\text{sol}}^{\text{ele}} + \Delta G_{\text{sol}}^{\text{nonpolar}} \quad (4)$$

where $\Delta G_{\text{sol}}^{\text{ele}}$ is the polar contribution to solvation and $\Delta G_{\text{sol}}^{\text{nonpolar}}$ is the nonpolar solvation term. The former component was calculated using the PB calculation, whereas the latter term is determined using Eq. (5):

$$\Delta G_{\text{sol}}^{\text{nonpolar}} = \gamma \text{SASA} + b \quad (5)$$

where SASA is the solvent-accessible surface area (\AA^2) and γ and b represent experimental solvation parameters.

The normal mode calculation is required to obtain the entropy, but it is time-consuming for large systems, considering the entropic differences among the systems is normally small when the receptors of all system models are quite similar, the entropy contribution of complexes was not considered in our ΔG calculations in order to save the computational cost; after all, our goal is to compare the binding energy of various ligands with the same receptor (as opposed to comparing the binding energies across receptors). The above binding energy calculations were carried out on the last 25 ns of each trajectory and the lowest binding energy for each complex was kept as a measure of the binding affinity.

3.7. Pharmacophore consensus model

The MD-retrieved representative binding conformations of ECG and EGCG were superposed using the Flexible Alignment algorithm of MOE v2012.10. The “rigid mode” was turned on to retain the molecules’ active configurations. After the superposition, unified types of pharmacophore features were generated using the consensus approach. A tolerance radius of 1.5Å and consensus score threshold of 75% were set to generate a consensus pharmacophore model.

The tolerance radius is the neighborhood distance threshold. Annotation points closer than this distance are considered to be neighbors. Neighborhoods determine in which regions of space the consensus score will be calculated. The consensus score is a measure of the proportion of molecular conformations represented in a set of annotation points; it represents the level of consensus among all input molecular conformations in a region of space. The regions are defined by neighborhoods of annotation points, as determined by the “tolerance” distance threshold. A group of annotation points will become a suggested feature only if: 1) it is composed of overlapping neighborhoods of annotation points, 2) the consensus score of each neighborhood exceeds the consensus score threshold, and 3) the consensus score of the entire group exceeds the consensus score threshold.⁴³ The features that achieve consensus score of 100% were marked as essential features. When employing the generated pharmacophore for virtual screening, the hits must match all the essential features at least.

4. Conclusion

In this study, our *in vitro* experiments have demonstrated that two major components of green tea polyphenols, ECG and EGCG, inhibit the three important enzymes (FPPS, MVK and MDD) of the mevalonate pathway, which are involved in the biosynthesis of

cholesterol *in vivo*. In contrast, the other two green tea components, EC and EGC, have no such effects. Molecular simulation studies demonstrate that ECG and EGCG interact with FPPS, MVK, and MDD at their triangular binding pockets with two types of pharmacophores.

From the perspective of receptors, their triangular binding pockets are quite similar in shape, and can accommodate ligands with three groups. Compounds fitting FPPS-class pharmacophore will selectively bind to FPPS; compounds fitting MVK-class pharmacophore will selectively bind to MVK; the pockets of MDD is relatively flexible compared to FPPS and MVK, and compounds fitting either pharmacophores will bind to MDD.

From the perspective of ligands, ECG and EGCG all have three groups: the core group, the two side groups A and B. These three groups can form strong and stable interactions with triangular binding pockets after some conformational changes. On the other hand, the polyphenols are relatively flexible, which is reflected by the dihedral between the A and B groups. This makes them suitable for all three triangular binding pockets of FPPS, MVK and MDD, although these three pockets are different. EC and EGC did not exhibit significant inhibitions to the three targets. The probable reason is that the scaffolds of EC and EGC lack galloyl groups (B groups) to form hydrogen bonds and π - π bonding interactions with the receptors. Consequently, neither EC nor EGC can fully occupy the triangular binding site to form stable pharmacophores with the receptors.

Insights from binding energy calculations, decompositions and binding mode analyses indicate the essential residues and their interactions with ligands. These essential interactions and residues should be important for designing new inhibitors against these three targets. The proposed pharmacophores may be utilized for further virtual screening and ligand design, although they may need simplifications. New agents that simultaneously inhibit FPPS, MVK, and MDD may provide more effective new

chemotherapy for hyperlipidemia.

Acknowledgements

This work was supported by a grant from the National High Technology Research and Development Program of China (863 Program) (No. 2012AA020307), the Guangdong Recruitment Program of Creative Research Groups (No. 2009010058), the National Natural Science Foundation of China (No. 81001372, 81173470, and 81274170), and the Special Funding Program for the National Supercomputer Center in Guangzhou (2012Y2-00048/2013Y2-00045, 201200000037) and Shenzhen. This research was also supported in part by Guangdong Innovative Research Team Program.

References

1. N. Khan and H. Mukhtar, *Life Sci.*, 2007, 81, 519-533.
2. A. B. Sharangi, *Food Res. Int.*, 2009, 42, 529-535.
3. H. N. Graham, *Prev. Med.*, 1992, 21, 334-350.
4. J. L. Bushman, *Nutr. Cancer*, 1998, 31, 151-159.
5. J. Blumberg, *The Journal of nutrition*, 2003, 133, 3244S-3246S.
6. C. S. Yang, X. Wang, G. Lu and S. C. Picinich, *Nat. Rev. Cancer*, 2009, 9, 429-439.
7. Y.-x. Zhu, H. Huang and Y.-y. Tu, *Int. J. Food Sci. Technol.*, 2006, 41, 333-340.
8. M. G. L. Hertog, E. J. M. Feskens, D. Kromhout, P. C. H. Hollman and M. B. Katan, *The Lancet*, 1993, 342, 1007-1011.
9. K. J. Mukamal, *Circulation*, 2002, 105, 2476-2481.
10. H. D. Sesso, J. M. Gaziano, J. E. Buring and C. H. Hennekens, *Am. J. Epidemiol.*, 1999, 149, 162-167.
11. S. Mandel, O. Weinreb, T. Amit and M. B. H. Youdim, *J. Neurochem.*, 2004, 88, 1555-1569.
12. Y. H. Kao, H. H. Chang, M. J. Lee and C. L. Chen, *Mol. Nutr. Food Res.*, 2006, 50, 188-210.

13. S. Wolfram, Y. Wang and F. Thielecke, *Mol. Nutr. Food Res.*, 2006, 50, 176-187.
14. J. K. Lin and S. Y. Lin-Shiau, *Mol. Nutr. Food Res.*, 2006, 50, 211-217.
15. S. Bérubé-Parent, C. Pelletier, J. Doré and A. Tremblay, *Br. J. Nutr.*, 2007, 94, 432.
16. L. G. C. N. Maron Dj and et al., *Arch. Intern. Med.*, 2003, 163, 1448-1453.
17. S. I. Koo and S. K. Noh, *J Nutr Biochem*, 2007, 18, 179-183.
18. M. J. Davies, J. T. Judd, D. J. Baer, B. A. Clevidence, D. R. Paul, A. J. Edwards, S. A. Wiseman, R. A. Muesing and S. C. Chen, *The Journal of nutrition*, 2003, 133, 3298S-3302S.
19. D. K. Singh, S. Banerjee and T. D. Porter, *J Nutr Biochem*, 2009, 20, 816-822.
20. B. P. Laden and T. D. Porter, *Nutrition Research*, 2001, 21, 747-753.
21. I. Buhaescu and H. Izzedine, *Clin. Biochem.*, 2007, 40, 575-584.
22. Z. Fu, M. Wang, D. Potter, H. M. Miziorko and J.-J. P. Kim, *J. Biol. Chem.*, 2002, 277, 18134-18142.
23. Y. K. Cho, S. E. Rios, J. J. P. Kim and H. M. Miziorko, *J. Biol. Chem.*, 2001, 276, 12573-12578.
24. S. M. Houten, J. Koster, G. J. Romeijn, J. Frenkel, M. Di Rocco, U. Caruso, P. Landrieu, R. I. Kelley, W. Kuis, B. T. Poll-The, K. M. Gibson, R. J. A. Wanders and H. R. Waterham, *Europ. J. Hum. Genet.*, 2001, 9, 253-259.
25. M. J. Toth, L. Huwyler and J. Park, *Prep. Biochem. Biotechnol.*, 1996, 26, 47-51.
26. D. Krepiy and H. M. Miziorko, Philadelphia, PA, 2004.
27. A. Michihara, M. Sawamura, Y. Yamori, K. Akasaki and H. Tsuji, *Biol. Pharm. Bull.*, 2003, 26, 1484-1486.
28. S. M. Jackson, J. Ericsson, J. E. Metherall and P. A. Edwards, *J. Lipid Res.*, 1996, 37, 1712-1721.
29. J. M. Rondeau, F. Bitsch, E. Bourgier, M. Geiser, R. Hemmig, M. Kroemer, S. Lehmann, P. Ramage, S. Rieffel, A. Strauss, J. R. Green and W. Jahnke, *Chemmedchem*, 2006, 1, 267-273.
30. A. Szkopinska, E. Swiezewska and F. Karst, *Biochem. Biophys. Res. Commun.*, 2000, 267, 473-477.
31. E. Kellenberger, J. Rodrigo, P. Muller and D. Rognan, *Proteins-Structure Function and Bioinformatics*, 2004, 57, 225-242.
32. J. Kirchmair, P. Markt, S. Distinto, G. Wolber and T. Langer, *J. Comput. Aided Mol. Des.*, 2008, 22, 213-228.
33. J. Fang, D. Huang, W. Zhao, H. Ge, H. B. Luo and J. Xu, *J. Chem. Inf. Model.*, 2011, 51, 1431-1438.
34. W. Zhao, Q. Gu, L. Wang, H. Ge, J. Li and J. Xu, *J. Chem. Inf. Model.*, 2011, 51, 2147-2155.
35. D. Huang, Q. Gu, H. Ge, J. Ye, N. K. Salam, A. Hagler, H. Chen and J. Xu, *J.*

- Chem. Inf. Model.*, 2012, 52, 1356-1366.
36. C. G. Wermuth, C. R. Ganellin, P. Lindberg and L. A. Mitscher, *Pure Appl. Chem.*, 1998, 70, 1129-1143.
 37. Q. Gu, J. Xu and L. Gu, *Molecules*, 2010, 15, 5031-5044.
 38. J. Gao, X. Chu, Y. Qiu, L. Wu, Y. Qiao, J. Wu and D. Li, *Chem. Commun. (Camb.)*, 2010, 46, 5340-5342.
 39. Y. Qiu and D. Li, *Biochim. Biophys. Acta*, 2006, 1760, 1080-1087.
 40. X. Chu and D. Li, *Protein Expression Purif.*, 2003, 27, 165-170.
 41. M. L. Colgrave and D. J. Craik, *Biochemistry*, 2004, 43, 5965-5975.
 42. T. A. Halgren, *J. Comput. Chem.*, 1996, 17, 490-519.
 43. MOE, Chemical Computing Group Inc., 1010 Sherbooke St. West, Suite #910, Montreal, QC, Canada, 2011.
 44. M. J. Frisch, G. W. Trucks, H. B. Schlegel, G. E. Scuseria, M. A. Robb, J. R. Cheeseman, G. Scalmani, V. Barone, B. Mennucci, G. A. Petersson, H. Nakatsuji, M. Caricato, X. Li, H. P. Hratchian, A. F. Izmaylov, J. Bloino, G. Zheng, J. L. Sonnenberg, M. Hada, M. Ehara, K. Toyota, R. Fukuda, J. Hasegawa, M. Ishida, T. Nakajima, Y. Honda, O. Kitao, H. Nakai, T. Vreven, J. A. Montgomery, J. E. Peralta, F. Ogliaro, M. Bearpark, J. J. Heyd, E. Brothers, K. N. Kudin, V. N. Staroverov, R. Kobayashi, J. Normand, K. Raghavachari, A. Rendell, J. C. Burant, S. S. Iyengar, J. Tomasi, M. Cossi, N. Rega, J. M. Millam, M. Klene, J. E. Knox, J. B. Cross, V. Bakken, C. Adamo, J. Jaramillo, R. Gomperts, R. E. Stratmann, O. Yazyev, A. J. Austin, R. Cammi, C. Pomelli, J. W. Ochterski, R. L. Martin, K. Morokuma, V. G. Zakrzewski, G. A. Voth, P. Salvador, J. J. Dannenberg, S. Dapprich, A. D. Daniels, Farkas, J. B. Foresman, J. V. Ortiz, J. Cioslowski and D. J. Fox, Wallingford CT, 2009, DOI: citeulike-article-id:9096580.
 45. J. Wang, W. Wang, P. A. Kollman and D. A. Case, *J. Mol. Graph. Model.*, 2006, 25, 247-260.
 46. W. L. Jorgensen, J. Chandrasekhar, J. D. Madura, R. W. Impey and M. L. Klein, *Comparison of simple potential functions for simulating liquid water*, AIP, 1983.
 47. D. A. Case, T. E. Cheatham, 3rd, T. Darden, H. Gohlke, R. Luo, K. M. Merz, Jr., A. Onufriev, C. Simmerling, B. Wang and R. J. Woods, *J. Comput. Chem.*, 2005, 26, 1668-1688.
 48. A. W. Gotz, M. J. Williamson, D. Xu, D. Poole, S. Le Grand and R. C. Walker, *J. Chem. Theory Comput.*, 2012, 8, 1542-1555.
 49. H. Ge, Y. Wang, C. Li, N. Chen, Y. Xie, M. Xu, Y. He, X. Gu, R. Wu, Q. Gu, L. Zeng and J. Xu, *J. Chem. Inf. Model.*, 2013, 53, 2757-2764.
 50. J.-P. Ryckaert, G. Ciccotti and H. J. C. Berendsen, *J. Comput. Phys.*, 1977, 23, 327-341.
 51. R. H. Zhou, E. Harder, H. F. Xu and B. J. Berne, *J. Chem. Phys.*, 2001, 115,

- 2348-2358.
52. B. R. Miller, T. D. McGee, J. M. Swails, N. Homeyer, H. Gohlke and A. E. Roitberg, *J. Chem. Theory Comput.*, 2012, 8, 3314-3321.
 53. T. Hou, J. Wang, Y. Li and W. Wang, *J. Chem. Inf. Model.*, 2011, 51, 69-82.